D M 21, 2008
Preprint typeset using LaTeX style emulateapj v. 10/09/06

# *CHAMPLANE* DEEP GALACTIC BULGE SURVEY. I. FAINT ACCRETION-DRIVEN BINARIES IN THE LIMITING WINDOW .

M B [1], J S H [1], J G [1], X K [1], S L [2], P Z [1]

*Draft version May 21, 2008*

## ABSTRACT

We have carried out a deep X-ray/optical survey with *Chandra* and *HST* of low-extinction regions in the Galactic bulge. Here we present the results of a search for low-luminosity ($L_X \lesssim 10^{34}$ erg s$^{-1}$) accreting binaries among the *Chandra* sources in the region closest the Galactic Center, at an angular offset of 1.5 degrees. Based on their blue optical colors and excess H$\alpha$ fluxes, we identify three to four probable compact binaries; these are most likely white dwarfs accreting from low-mass companions in cataclysmic variables (CVs) although we cannot exclude that they are quiscent neutron-star or black-hole low-mass X-ray binaries. Our distance estimates put these systems at $\gtrsim$2 kpc and we use this to investigate the CV space density in the bulge. The X-ray properties of two likely CVs are similar to those of the faint and hard X-ray sources in the Galactic-Center region that are associated with magnetic CVs; if our candidates belong to the same population, they would be the first members to be optically identified. Based on their small H$\alpha$-excess fluxes or high X-ray–to–optical flux ratios, we find 23 more marginal candidate accreting binaries, some of which show indications of being intrinsically absorbed; however, their properties can also be explained if they are dMe stars or active galaxies.

*Subject headings:* X-rays: binaries — X-rays: stars — Galaxy: bulge

## 1. INTRODUCTION

With its sharp view, the *Chandra* X-ray Observatory has revealed a large population of X-ray point sources in the central 40 pc of our Galaxy (Muno et al. 2003). The majority of these are faint ($L_X \approx 10^{31-34}$ erg s$^{-1}$) and intrinsically hard; comparison with the X-ray properties of candidate local analogs suggests that the Galactic-Center sources are a mix of compact objects (white dwarfs, neutron stars and black holes) accreting from close companions. From the lack of a significant fraction of these sources with bright ($K < 15$) infrared counterparts, Laycock et al. (2005) excluded that the contribution of neutron stars in wind-fed Be high-mass X-ray binaries exceeds ~10% (as suggested by Pfahl et al. (2002)), leaving magnetic white dwarfs accreting from low-mass companions (i.e. magnetic cataclysmic variables (CVs)) as the most likely dominating source class. This also leaves us with an enormous challenge to identify these sources at other wavelenghts: CVs in the Galactic Center are too faint to be detected in the infrared (unless they undergo a nova or bright dwarf-nova outburst), and the Galactic-Center region is too heavily obscured by dust to search for counterparts in the optical. At the same time, by the sheer number of Galactic-Center X-ray sources (thousands), this population has great importance for understanding the Galactic accreting binary content and unraveling the evolutionary history of the inner Galaxy.

As part of the *Chandra* Multi-wavelength Plane survey (*ChaMPlane*; Grindlay et al. 2005), we have carried out an X-ray/optical survey of deep, near-simultaneous *Chandra* and *HST* pointings of three low-extinction regions, or *Windows*, in the Galactic bulge. These *Windows* lie on a nearly radial alignment with the Galactic Center, at angular offsets between 1.5° and 4°. One of the aims of this survey is to look for signatures of a population of faint, hard X-ray sources similar to the one found by Muno et al. (2003), and take advantage of the more favorable conditions for source identification compared to the Galactic Center. Indeed, based on the X-ray analysis of these three and four more deep *Chandra* fields in the inner bulge, Hong et al. (2008) (H08) show that the faint and hard population can be traced out to at least 1.5° from the Galactic Center, i.e. out to our "innermost" *Window*. We have named this field the *Limiting Window* (*LW*) because extinction rapidly increases (and therefore chances for optical identification drastically decline) when moving closer to the Galactic Center. In this paper we try to identify X-ray binaries (that will be most likely CVs given their relative abundance) among *Chandra* sources in *LW* by searching for optical counterparts; by extrapolation, this could also constrain the nature of the faint, hard Galactic-Center sources found by Muno et al. (2003).

Another main goal of our *Windows* survey is to study for the first time the population of CVs, i.e. the most common class of low-luminosity accreting binaries with compact objects, at large distances from us. Much of what we know about the Galactic CV population is based on a sample of relatively local systems, mainly within ~2 kpc from the Sun (see, for example, Ak et al. (2008), Warner (1995)). Our deep *Chandra* exposures have the sensitivity to detect bright ($L_X \gtrsim 10^{31}$ erg s$^{-1}$) CVs at $\gtrsim$8 kpc, which means we can significantly increase the depth of existing CV samples. In a follow-up paper we will combine our results with the search for CVs and other accreting binaries in Baade's and Stanek's *Windows* (initial results were already given in van den Berg et al. (2006)). Subsequent papers will discuss stellar coronal sources.

After describing the X-ray and optical observations in §2, we outline the analysis steps in §3. We present the identified candidate CVs in §4, and discuss our results in the contexts of the Galactic CV population and the Galactic-Center X-ray–source population in §5. We end with our conclusions in §6.

## 2. OBSERVATIONS

### 2.1. *Chandra data*

The *Limiting Window* was observed for 100 ks with the *Chandra*/ACIS-I aimpoint placed at ($l$,$b$)=(0$^{\rm d}$.10,−1$^{\rm d}$.43). Due to observatory constraints, the observation was split in three

[1] Harvard-Smithsonian Center for Astrophysics, 60 Garden Street, Cambridge, MA 02138, USA; maureen@head.cfa.harvard.edu
[2] Gemini Observatory, Hilo, HI, USA

exposures: ObsID 6362 (2005 Aug 19, 38 ks), ObsID 5934 (2005 Aug 22, 41 ks) and ObsID 6365 (2005 Oct 25, 21 ks). We stacked the three images into a single image; in the remainder of the paper we only consider the stacked pointing. The data were processed with the *ChaMPlane* X-ray data-reduction pipeline (Hong et al. 2005). We performed source detection on images in a soft (0.3–2.5 keV), hard (2.5–8.0 keV) and broad (0.3–8.0 keV) energy band, and merged the resulting source lists into a master source catalog following the procedures described in H08. A total of 325 valid ACIS-I sources are detected. The pipeline produces source positions and corresponding 95% confidence radii $r_{95}$, net source counts (0.3–8.0 keV) extracted from a region enclosing 95% of the energy at 1.5 keV, and energy quantiles $E_x$ where $E_x$ is the energy below which $x$% of the counts in the 0.3–8.0 keV band are detected. We use the latter to constrain X-ray spectral parameters for low-count sources; see Hong et al. (2004) for a description of the quantile method.

### 2.2. *HST/ACS data*

*HST* observed the inner area of the ACIS field with a 2×2 mosaic of slightly overlapping pointings of the Wide Field Camera (WFC) on the Advanced Camera for Surveys (ACS). The observations (program GO-10353) were carried out simultaneous with the first *Chandra* exposure (2005 Aug 19). The WFC images a $3'.4\times3'.4$ field with $\sim0''.05$ pixels using two CCD detectors separated by a $2''.5$ gap. Exposures were taken through the F435W ("$B_{435}$"), F625W ("$R_{625}$", similar to Sloan $r$) and F658N (H$\alpha$) filters. Each tile of the mosaic was observed with the same exposure sequence: 4×492 s in F435W, 168 s + 2×167 s in F625W and 4×496 s + 4×492 s in F658N. The offsets in Galactic coordinates $\Delta l, \Delta b$ (in degrees) of each *HST* pointing from the center of the *Chandra* pointing are (−0.04,+0.01), (+0.04,−0.01), (+0.01,+0.04) and (−0.01,−0.04). No dithering was applied to fill in the WFC chip gap. After boresight correction (see §3.5), 100 *Chandra* sources are included in the field-of-view of the ACS mosaic, including one source whose 95% X-ray error circle lies partially in the chip gap.

## 3. ANALYSIS

### 3.1. *ACS photometry*

Photometry is performed using the stellar-photometry package DOLPHOT[3], a modified version of the HSTphot package to do photometry on *HST*/WFPC2 images (Dolphin 2000). We run DOLPHOT on the $B_{435}$, $R_{625}$ and H$\alpha$ images separately in the point-spread-function (PSF) fitting mode, in which filter-dependent model PSFs are used as initial guesses for the actual PSFs of the images being analyzed; the latter are slightly adjusted using isolated stars which is necessary to correct for observation-specific focus and/or thermal conditions of the telescope. For stars with a signal-to-noise ratio (SNR) <10 aperture photometry is used. Source detection is run twice, with sources detected in the first pass removed during the second pass. Then, for each star, a photometric solution is iteratively derived with the sky and neighbors subtracted until the photometry of the star and its neighbors converge to a stable solution. Sources that are separated by <2 pixels are merged into a single source.

DOLPHOT runs on the distorted (`flt`) images to avoid errors associated with the pixel resampling that is necessary to correct for the significant geometric distortion of ACS. The resulting output catalog, however, is aligned to a distortion-corrected (`drz`) image constructed with the STScI task *multidrizzle*. Optical source catalogs are derived for each filter separately; these are combined using a match criterion of a maximum separation of 1.5 pixels. DOLPHOT produces magnitudes that are corrected for charge-transfer–efficiency degradation and that correspond to a 4-pixel aperture. We compute a filter-dependent aperture correction to 10 pixels (between −0.08 and −0.10 mag) using aperture photometry of a few isolated stars; together with the aperture corrections from 10 pixels to "infinity" (Sirianni et al. 2005) these are applied to the DOLPHOT magnitudes to obtain calibrated photometry. Zeropoint offsets are applied to express the final magnitudes in the STMAG system. The approximate detection limits for SNR=5 are $B_{435} \approx 27$, $R_{625} \approx 26.5$, and $H\alpha \approx 25.5$.

In an attempt to remove artifacts and non-stellar objects from the source list, we generally only consider stars with $\chi^2 \leq 3$, SNR≥5, sharpness ≤±0.5, error flags < 8 and object classifications appropriate for stellar sources (type < 2); see the DOLPHOT manual for details. Even after applying these criteria, the final source list is not guaranteed to be free of artifacts. For example, in the $R_{625}$ versus $B_{435} - R_{625}$ color-magnitude diagram (CMD) a small group ($\lesssim$ 2% of the total number of sources detected in all three bands) of faint, blue sources ($R_{625} > 22.5, B_{435} - R_{625} < 2$) is prominent, that upon closer inspection turn out to be mostly associated with PSF artifacts near very bright stars. For the CMDs and color-color diagrams (CCDs) presented in this paper, in which we have plotted sources from only one of the ACS chips for clarity, we have manually cleaned this region of the CMD from artifacts. For the identification of candidate counterparts to *Chandra* sources, we visually examine all detections in the search area (§3.5) to check that no valid optical source is erroneously eliminated and that no artifact is mistaken for a real source.

### 3.2. *Improvement of the HST absolute astrometry*

The coordinates in the optical catalogs are corrected for geometric distortion but the *HST* absolute astrometry can be off by up to $3''$ (see for example Koekemoer et al. 2005). To improve the astrometric accuracy, we tie the optical astrometry to the International Celestial Reference System (ICRS) using stars in the UCAC2 catalog that have a positional accuracy $\lesssim0''.070$ (Zacharias et al. 2004). Since UCAC2 stars are bright (and thus often saturated) and scarce in the ACS images, we use a ground-based $V$-band image of *LW* to derive secondary astrometric standards as an intermediate step. The ground-based images were obtained with the CTIO-4m Mosaic camera (field-of-view $36'\times36'$) and were reduced following the procedures described in Zhao et al. (2005).

An astrometric solution is first derived for a section of the Mosaic image that includes the full ACS mosaic using 132 UCAC2 stars. Fitting for shift, rotation angle, scale factor and distortions results in a solution with rms residuals of $0''.040$ in right ascension and $0''.036$ in declination. Next, the solution is transferred to one image of each ACS pointing using sets of ~200 secondary standards selected from unsaturated and relatively isolated stars in the Mosaic and ACS images; we choose the stacked F658N images for this purpose that should be clean of cosmic rays and other artifacts given the large number of individual exposures. The resulting fits for shift, rotation angle and scale factor have rms residuals of, typically, $0''.02$ in both right ascension and declination. Fi-

[3] http://purcell.as.arizona.edu/dolphot

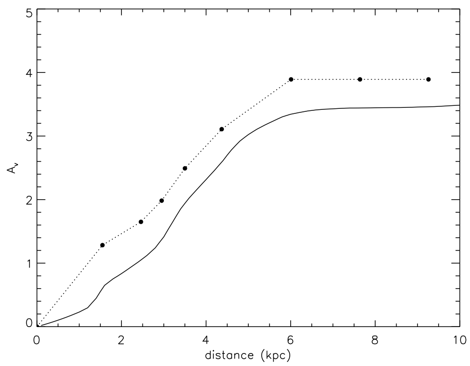


F . 1.— Extinction $A_V$ as function of distance as predicted by D03 (solid line) and M06 (dotted line). For the latter, we have assumed $A_V$=8.3$A_{Ks}$ (M06).

nally, the solutions are transferred to all ACS images of a given pointing using ∼2000 tertiary standards; the associated errors are negligible. We estimate the final 1$\sigma$ accuracy of the optical absolute astrometry ($\sigma_o$) as the quadratic sum of the errors in the UCAC2 astrometry, the UCAC2–Mosaic tie and the Mosaic–*HST* tie, i.e. 0.″090–0.″095. We adopt a uniform value of 0.″095 for all pointings.

### 3.3. *Extinction*

Extinction along the line of sight towards *LW* is relatively low for a bulge field but not entirely negligible, and needs to be considered in order to derive intrinsic (unabsorbed) X-ray and optical fluxes. In Fig. 1 we compare two estimates from the literature of the extinction as function of distance. The three-dimensional $A_V$ maps by Drimmel et al. (2003) (D03) are based on a model for the Galactic dust distribution but rescaled to match COBE far-infrared data; the maps are thus limited to a resolution of ∼0.35°×0.35°. For the direction of *LW*, D03 predict that the bulk of absorbing material lies in front of 6 kpc after which $A_V$ levels off to 3.8; this includes a ∼10%-contribution from material that lies mainly beyond 10 kpc. However, for $|l| < 20°$ the underlying dust model is not accurate. The $A_{Ks}$ extinction maps by Marshall et al. (2006), available for the inner Galaxy at 15′ resolution and computed out to ∼9 kpc, are derived by comparing the intrinsic colors of late-type giants with their observed 2MASS colors. The maximum predicted extinction towards *LW* is somewhat higher than the value from D03 ($A_V$=3.9 at 8 kpc for M06 versus $A_V$=3.5 for D03), although both curves have very similar shapes. For the total integrated extinction, we will adopt the value from D03 but scaled to match $A_V$ from M06 at 8 kpc, i.e. $A_V$ = 4.2; this corresponds to a neutral-hydrogen column density $n_H$=7.6 $10^{21}$ cm$^{-2}$ (Predehl & Schmitt 1995).

### 3.4. *X-ray spectral properties*

All sources in *LW* but one have fewer than 100 counts (the brightest source, our CV candidate X 1 (§4.1.1), has 152 net counts); since this precludes the use of spectral fitting, we resort to quantile analysis (Hong et al. 2004) to derive the X-ray spectral properties of our sample. In summary, quantile analysis constrains the spectral parameters and column density from comparing the observed energy quantiles to those expected for a spectral model of choice; in the *ChaMPlane* analysis, we use the 25%, 50% and 75% energy quantiles.

TABLE 1

S

| group | model | parameter | $n_H$ (atoms cm$^{-2}$) |
|---|---|---|---|
| 0 | MeKaL | $kT$ = 1 keV | 0.76 |
| 1 | power law | Γ=1.28 | 0.76 |
| 2 | power law | Γ=1.21 | 1.95 |

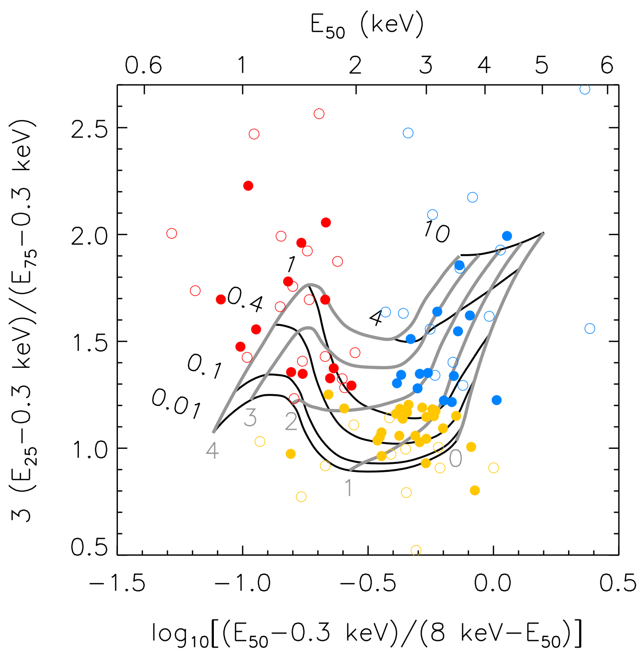


F . 2.— Quantile color-color diagram showing the *Chandra* sources in the ACS field-of-view and their X-ray spectral classification. For reference, we plot a grid for a power-law spectral model. The spectral properties of a source can be derived from its location with respect to the grid: thick grey lines indicate contours of constant $n_H$ while Γ is fixed along the black lines. Sources in the three spectral classes are plotted in red (group 0; soft sources), yellow (group 1; relatively hard sources) and blue (group 2; relatively hard and absorbed sources). Sources with more and fewer than 15 net counts are plotted with filled and open symbols, respectively.

Since measurement errors on the quantiles of individual sources sometimes allow a broad range of parameters, we divide the sources in three spectral classes and assign to all sources of a given class one spectral model and $n_H$ based on the quantiles of their stacked counts. H08 describe in detail the process of assigning spectral classes. The H08 spectral classification that we use in this paper is represented in Fig. 2. For the soft group (group 0), we assume that the X-ray spectra can be characterized by a 1-keV MeKaL model which describes emission of an optically-thin hot plasma, appropriate for the coronal emission of normal late-type stars; the maximum $n_H$ along the line of sight from §3.3 is adopted. For the hard group (1) we use the spectral parameters from H08 with a small adjustment, viz. instead of the quantile-based $n_H$, we use the integrated $n_H$ from §3.3 (≲5% difference). Parameters for the hard and absorbed group (2) are taken from H08 without adjustment. The parameters for each spectral class are summarized in Table 1. To minimize the effect of an incorrect choice of $n_H$ (not all sources are seen through the maximum column density along the line of sight) we avoid using fluxes in the soft band. Since not all sources are detected in the hard band ($Hc$=2.0–8.0 keV), we compromise by working with broad-band ($B_x$=0.3–8 keV) fluxes.

### 3.5. *Boresight correction and optical identification*

We improve the absolute astrometry of the *Chandra* positions (90%-uncertainty is 0.″6) by identifying likely matches between X-ray and optical sources. For this initial search for counterparts we use a search area that corresponds to a $2\sigma$ match radius where $\sigma$ is the quadratic sum of $\sigma_x$ (the error on the X-ray positions, i.e. $r_{95}$ normalized to $1\sigma$) and $\sigma_o$ (the error on the optical positions, see §3.2). We accept an optical source as a likely counterpart if it has unusual optical colors (blue, red and/or with an H$\alpha$ excess with respect to the bulk of optical sources with similar optical magnitudes) or if it has optical and X-ray colors and an X-ray–to–optical flux ratio consistent with normal foreground stars (only if there are no other contenders in the error circle). We also include matches with OGLE-III variables (A. Udalski, private communication) that can be unambiguously identified in the *HST* images and are unsaturated (saturation hampers the determination of accurate optical positions); the properties of these variables are the topic of a forthcoming paper.

After the first round of matching, an initial boresight is determined from the weighted (by $r_{95}$) average of the X-ray minus optical positions of the likely matches. A uniform offset is determined for all four ACS pointings since their astrometries have been put on the same system; this is verified by examining the area where the pointings overlap. After correcting the X-ray positions for the boresight, the matching is repeated with $\sigma$ updated to the quadratic sum of $\sigma_x$, $\sigma_o$ and $\sigma_b$ where the latter is the boresight error. The resulting final boresight is almost negligible: $\Delta\alpha$=−0.02±0.05, $\Delta\delta$=+0.05±0.04 (based on 11 matches).

## 4. RESULTS

At least one astrometric optical match is found for each of the 100 *Chandra* sources; for the majority (~90%), multiple candidate optical counterparts lie within the $2\sigma$ match radius (0.″67 on average). We mainly consider the optical colors of these candidates, together with the ratio of the X-ray and optical fluxes ($f_{Bx}/f_{R_{625}}$ or $f_{Bx}/f_R$ in brief) and the X-ray spectral properties to constrain which of them (if any) is the most likely counterpart. We present cases that we have identified as plausible and possible CVs (or other accreting binaries) in §4.1. Additional identifications are briefly discussed in §4.2; the main purpose here is to compare the X-ray properties of the candidate CVs with those of other source classes. Constraints on the nature of the hard point sources in *LW* are discussed in §4.3.

### 4.1. *Candidate accreting binaries*

#### 4.1.1. *Selection based on optical colors*

The optical spectra of most CVs show Balmer emission lines from an accretion disk or stream. Therefore, if a *Chandra* source can be matched with a blue optical source that also has excess H$\alpha$ flux, the source is a likely CV. We thus find four prime CV candidates; Fig. 3 shows the locations of their counterparts in the $R_{625}$ versus $B_{435}-R_{625}$ and $R_{625}$ versus H$\alpha-R_{625}$ CMDs, labelled with X 1 to X 4. In the *LW* field however, where we see sources through a range of foreground extinctions, the interpretation of optical colors is not straightforward: as we show below using the CCDs in Fig. 4, a distant CV can be confused with a nearby late-type star.

First we compare the observed optical colors of X 1 to X 4 to those expected for CVs which we have simulated with a spectrum with a flux-wavelength dependence $F \propto \lambda^{-2/3}$, i.e. appropriate for the emission from an accretion disk (Drew et al. 2005). The grid in Fig. 4a shows how these synthetic colors behave as a function of reddening $E(B-V)$ and equivalent width (EW) of the H$\alpha$ line. For this particular spectrum and the adopted maximum extinction towards *LW* ($E(B-V)$=1.35), no CVs are expected with $B_{435}$–$R_{625}\gtrsim$1.2; however, different assumptions for the underlying optical spectrum (e.g. a contribution from the light of the secondary, small-scale variations in the foreground extinction and internal absorption in the binary itself) can explain redder systems like X 1 and X 3. The location of the unreddened main sequence is plotted in blue; this illustrates how our color-selection of CV candidates can cause confusion with nearby unreddened or moderately reddened M dwarfs—also common X-ray sources. The color grid for an M0 dwarf in Fig. 4b shows this in more detail; for example, the optical colors of X 4 could point at a CV with $E(B-V)\approx$1.4 and EW(H$\alpha$)≈30–40Å, but can in principle also be explained by an M2–3 dwarf with $E(B-V)\approx$0 and EW(H$\alpha$)≈10Å. X 4 is unlikely to be of later spectral type (the source is too blue) or of earlier type since this would require that EW(H$\alpha$)≳15Å. In the spectroscopic study of X-ray selected M-dwarfs by Mochnacki et al. (2002), the equivalent width of H$\alpha$ does not exceed 11 Å among the 54 stars in the sample.

We try to resolve this ambiguity by invoking other properties in addition to optical colors. For X 1 and X 3, their classification as CVs is the more plausible one on the basis of their X-ray colors; the quantile diagram of Fig. 5 shows that their spectra are hard ($kT$>10 keV or $\Gamma\gtrsim$1) which is unusual for stellar coronal sources even during strong flares (Osten et al. 2008). Also for X 4, which is softer in X-rays, we favor the explanation as CV: the absolute magnitude and $V-R$ color of an M2 dwarf would put this star at a distance of ~3.5–4 kpc, which is inconsistent with the implied low reddening from Fig. 4b. Additionaly, our estimate for the ratio of its intrinsic X-ray to optical flux (equal to the observed value if $E(B-V)\approx$0, i.e. log $f_{Bx}/f_R$=−0.0(2)) is high compared to the typical range observed for active M dwarfs (see Sect. 4.1.2). The case of X 2 is less clear. If the source is an M5 dwarf with EW(H$\alpha$)≈10Å, its distance would be ~1–1.5 kpc and thus $E(B-V)\approx$0.15–0.3 which (given the uncertainty of the distance versus $A_V$ curves) is roughly consistent with the estimated $E(B-V)$ from Fig. 4. Moreover, the soft spectrum of X 2 (Fig. 5) is more typical for coronal than accreting sources. We conclude that of our four blue and H$\alpha$-excess sources, X 1, X 3 and X 4 are plausible CVs while X 2 is a possible CV but alternatively a dMe star. We present the red and blue finding charts of these candidates in Fig. 6 and summarize their main properties in Table 2.

An additional twelve *Chandra* sources are matched with optical sources that have small H$\alpha$-excesses but are not or only slightly blue compared to the bulk of the optical sources, or for which the blue magnitude has SNR<5; these are marked with green diamonds in Fig. 4 and included in Table 2 as X 5–X 16. Whereas the lack of blue colors is perhaps more suggestive of them being late-type stars rather than CVs, the X-ray colors of some of these do not support this interpretation (see Fig. 5). In particular, X 12 and X 15 (the bluest of the group) are relatively hard, although we use caution in interpreting their quantile values given the small number of counts. The X-ray spectra of X 8, X 10, X 11, X 14 and possibly X 5 are absorbed, with $n_H\gtrsim$1 $10^{22}$ cm$^{-2}$ ($A_V\gtrsim$5.6). This requires some source of extra extinction, for example originat-

TABLE 2

C

| ID | CXOPSJ... | counts | $E_{50}$ (keV) | RA(J2000) | Dec(J2000) | $R_{625}$ | $B_{435}$ | H$\alpha$ | $\log(f_{Bx}/f_R)$ | $\log(f_{Bx}/f_R)_u$ | group |
|---|---|---|---|---|---|---|---|---|---|---|---|
| X 1 | 175120.9-293318 | 152(14) | 3.0(2) | 267.837133 | −29.555124 | 23.76(3) | 25.44(6) | 23.47(4) | 1.37(4) | 0.07(4) | 1 |
| X 2 | 175118.1-293332 | 9(5) | 1.5(3) | 267.825739 | −29.558968 | 21.368(7) | 22.97(1) | 20.816(8) | −1.3(2) | −2.1(2) | 0 |
| X 3 | 175124.1-293738 | 14(6) | 1.8(3) | 267.850518 | −29.627499 | 22.30(1) | 24.06(3) | 22.07(2) | 0.53(6) | −0.78(6) | 1 |
| X 4 | 175140.0-293557 | 76(10) | 2.9(3) | 267.916749 | −29.599335 | 23.81(3) | 25.03(5) | 23.36(4) | 0.0(2) | −0.8(2) | 0 |
| X 5 | 175142.0-293401 | 21(6) | 2.9(6) | 267.925023 | −29.567146 | 24.54(4) | 27.0(3) | 24.32(8) | 0.9(1) | −2.6(1) | 2 |
| X 6 | 175140.2-293318 | 16(6) | 1.7(5) | 267.917938 | −29.555213 | 25.07(6) | 28.0(7) | 24.8(1) | 0.5(2) | −0.3(2) | 0 |
| X 7 | 175122.8-293514 | 12(5) | 1.1(3) | 267.845013 | −29.587301 | 22.82(2) | 25.29(6) | 22.45(2) | −0.1(2) | −1.4(2) | 1 |
| X 8 | 175111.8-293259 | 45(8) | 3.7(2) | 267.799330 | −29.549927 | 23.56(3) | 26.6(2) | 23.25(3) | 0.87(8) | −2.64(8) | 2 |
| X 9 | 175124.1-293756 | 29(7) | 1.3(1) | 267.850637 | −29.632244 | 21.521(8) | 23.79(2) | 21.29(1) | −0.7(1) | −1.5(1) | 0 |
| X 10 | 175118.7-293811 | 32(7) | 3.5(4) | 267.828270 | −29.636452 | 22.66(1) | 25.51(7) | 22.41(2) | 0.3(1) | −3.2(1) | 2 |
| X 11 | 175118.5-293732 | 15(6) | 3.1(3) | 267.827307 | −29.625596 | 23.92(3) | 26.9(2) | 23.66(5) | 0.5(2) | −3.0(2) | 2 |
| X 12 | 175115.8-293802 | 7(5) | 2.7(1.6) | 267.816065 | −29.634251 | 23.37(2) | 26.7(2) | 22.93(3) | −0.1(3) | −1.4(3) | 1 |
| X 13 | 175138.2-293658 | 14(6) | 1.4(2) | 267.907820 | −29.615469 | 22.58(2) | 24.76(5) | 22.38(2) | −0.6(2) | −1.4(2) | 0 |
| X 14 | 175134.8-293809 | 36(7) | 3.6(3) | 267.895200 | −29.636073 | 23.19(2) | 26.0(1) | 22.94(3) | 0.61(9) | −2.90(9) | 2 |
| X 15 | 175141.4-293508 | 16(6) | 2.3(9) | 267.922749 | −29.585738 | 22.82(2) | 24.93(5) | 22.65(2) | −0.0(2) | −1.3(2) | 1 |
| X 16 | 175142.8-293734 | 3(4) | 0.5(1.1) | 267.928849 | −29.626611 | 24.51(4) | 27.1(3) | 24.22(8) | −0.5(7) | −1.3(7) | 0 |

Errors in the absolute astrometry of the optical positions are ~0.″095. $\log(f_{Bx}/f_R)$ and $\log(f_{Bx}/f_R))u$ are the ratios of the observed and intrinsic X-ray and optical fluxes. Fluxes are corrected for extinction using the group-specific $n_H$ values (Table 1). Quoted errors in the flux ratios only include a contribution from errors in the X-ray counts, not any systematic errors.

ing inside the binary system or provided by the host galaxy of an AGN. The former option is further discussed §5.3, while in the latter case the H$\alpha$ excess could be explained if an emission line happens to be redshifted in the F65N band. For coronal sources such high $n_H$ values are not expected. Occasionaly, the column density is enhanced when a star undergoes a large coronal flare but these cases are rare and not yet fully understood (Güdel 2004). While we consider the remaining H$\alpha$-excess–only sources as marginal CV candidates, we include them all in Table 2 for completeness.

#### 4.1.2. *Selection based on $f_{Bx}/f_R$ ratios*

It is well-known (e.g. Stocke et al. 1991; Krautter et al. 1999) that the distribution of the ratio of intrinsic X-ray to optical fluxes for accreting binaries extends to significantly higher values[4] than for coronal sources, whereas it largely overlaps with the range observed for galaxies. Therefore, even in the absence of any optical matches with distinct optical colors, we can identify CV (or AGN) candidates among the *Chandra* sources by considering the minimum value of $f_{Bx}/f_R$ that results from the brightest optical source in the search area. The difficulty of applying this diagnostic to our sample is that we only have a rough estimate of the extinction that is needed to correct observed fluxes to intrinsic fluxes; the maximum extinction towards *LW* is sufficiently large to allow a large, and sometimes hardly constraining, range on $f_{Bx}/f_R$. We use the $n_H$ value appropriate for the quantile spectral class (Table 1) to correct the X-ray and optical fluxes but stress that this is only a rough estimate, especially for group=2 sources. We also assume that $f_V \approx f_R$, which facilitates comparison with the literature.

Among single stars, active M dwarfs have the highest values of $\log f_X/f_V$. The nearby sample from Schmitt & Liefke (2004) has $(\log f_x/f_V)_{\max} \approx -1$ in the ROSAT band which, for the X-ray spectra typical for coronal sources, would give a similar value in our $B_x$ band. Krautter et al. (1999) find $<\log f_x/f_V> = +1.33 \pm 0.50$ for dMe stars with a few outliers that have $\log f_x/f_V > -0.5$ (ROSAT band). For the active binaries discussed by Dempsey et al. (1993); Dempsey et al. (1997), $\log f_X/f_V$ does not exceed −1.3 (ROSAT band). Based on these ranges, we select possible CVs as sources with an intrinsic minimum $\log f_{Bx}/f_R > -1$. These eleven sources are listed in Table 3 and marked in the quantile color-color diagrams of 4. The relatively hard spectra support their classification as non-coronal sources but both their quantile values as their $f_{Bx}/f_R$ values prevent any distinction from AGN. Also the colors of the astrometric optical matches give no additional constraints on the source classifications. It is possible that the true optical counterparts are too faint to be detected. The detection limit of $R_{625} \approx 26.5$, implies that any undetected counterparts would have at least $\log f_{Bx}/f_R$ between +0.1 and +0.9 for the sources in Table 3 which is still consistent with accreting binaries.

[4] The CVs in Verbunt et al. (1997) span a range in $\log f_X/f_V$ from −2.7 to +0.7 where we converted from their 0.5–2.5 keV to our $B_x$ band using the 2 keV thermal-bremsstrahlung model used in Verbunt et al. (1997). The flux ratios are higher for harder spectra.

TABLE 3

C $f_{Bx}/f_R$

| ID | CXOPSJ... | counts | $E_{50}$ (keV) | $\log(f_{Bx}/f_R)$ (minimum) | $\log(f_{Bx}/f_R)_u$ (minimum) |
|---|---|---|---|---|---|
| X 16 | 175127.9-293508 | 14(5) | 2.4(6) | 0.9(2) | −0.4(2) |
| X 17 | 175119.1-293740 | 41(8) | 3.1(6) | 1.66(9) | 0.36(9) |
| X 18 | 175127.0-293706 | 46(8) | 2.6(5) | 1.37(8) | 0.06(8) |
| X 19 | 175130.0-293613 | 88(11) | 2.9(3) | 0.94(5) | −0.37(5) |
| X 20 | 175114.2-293224 | 22(7) | 3(1) | 1.1(1) | −0.2(1) |
| X 21 | 175133.6-293313 | 77(10) | 3.1(2) | 0.50(6) | −0.81(6) |
| X 22 | 175130.7-293232 | 54(9) | 3.2(3) | 0.65(7) | −0.65(7) |
| X 23 | 175120.7-293417 | 18(6) | 3.8(9) | 0.4(1) | −0.9(1) |
| X 24 | 175124.0-293532 | 13(5) | 1.2(7) | 0.6(2) | −0.7(2) |
| X 25 | 175139.6-293811 | 34(7) | 2.3(5) | 0.5(1) | −0.8(1) |
| X 26 | 175128.9-293412 | 14(6) | 2.7(7) | 0.6(2) | −0.7(2) |

$\log(f_{Bx}/f_R)$ and $\log(f_{Bx}/f_R))u$ are the ratios of the observed and intrinsic X-ray and optical fluxes. All sources have quantile spectral class 1; optical and X-ray fluxes are therefore dereddened with the appropriate $n_H$ value i.e. 7.6 $10^{21}$ cm$^{-2}$. Quoted errors in the flux ratios only include a contribution from errors in the X-ray counts, not any systematic errors.

#### 4.2. *Other identifications*

We defer the detailed discussion of coronal *LW* sources to a follow-up paper, but for the purpose of putting the X-ray properties of our candidate CVs into a broader context we include likely coronal sources in the quantile diagram of Fig. 5. Three sources are matched with very bright optical sources includ-

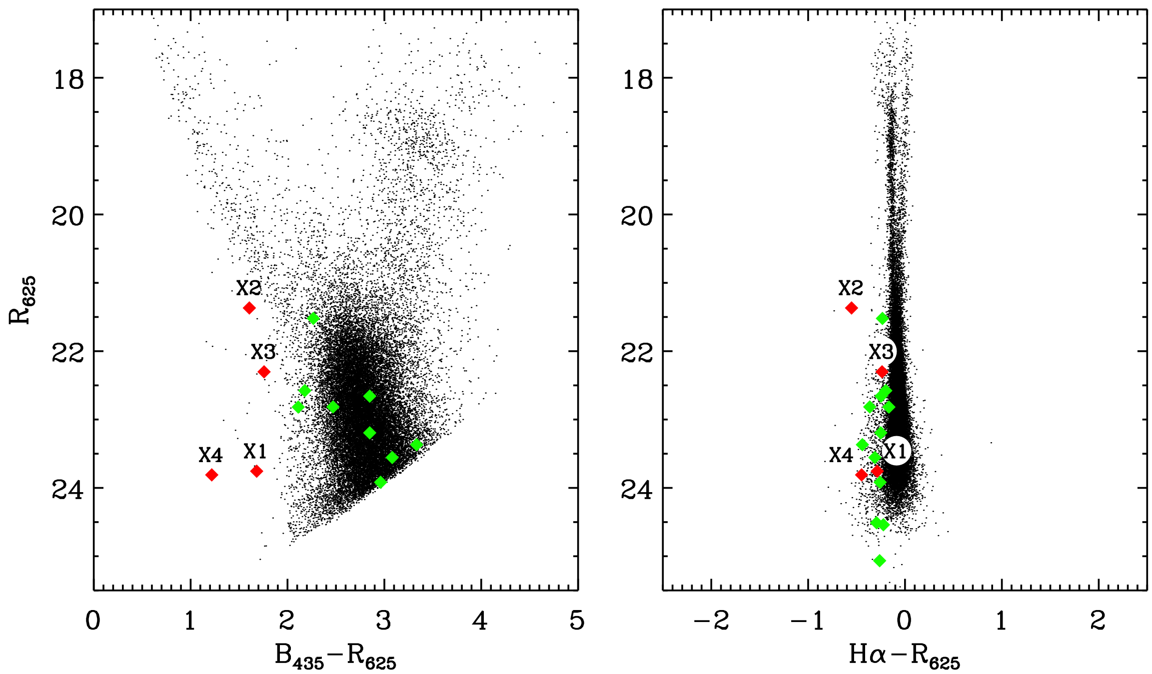


F . 3.— Color-magnitude diagrams with the candidate CVs from Table 2 indicated with red and green diamonds; only the best candidates are labelled. Candidates for which SNR<5 in F435W are not plotted in the left figure.

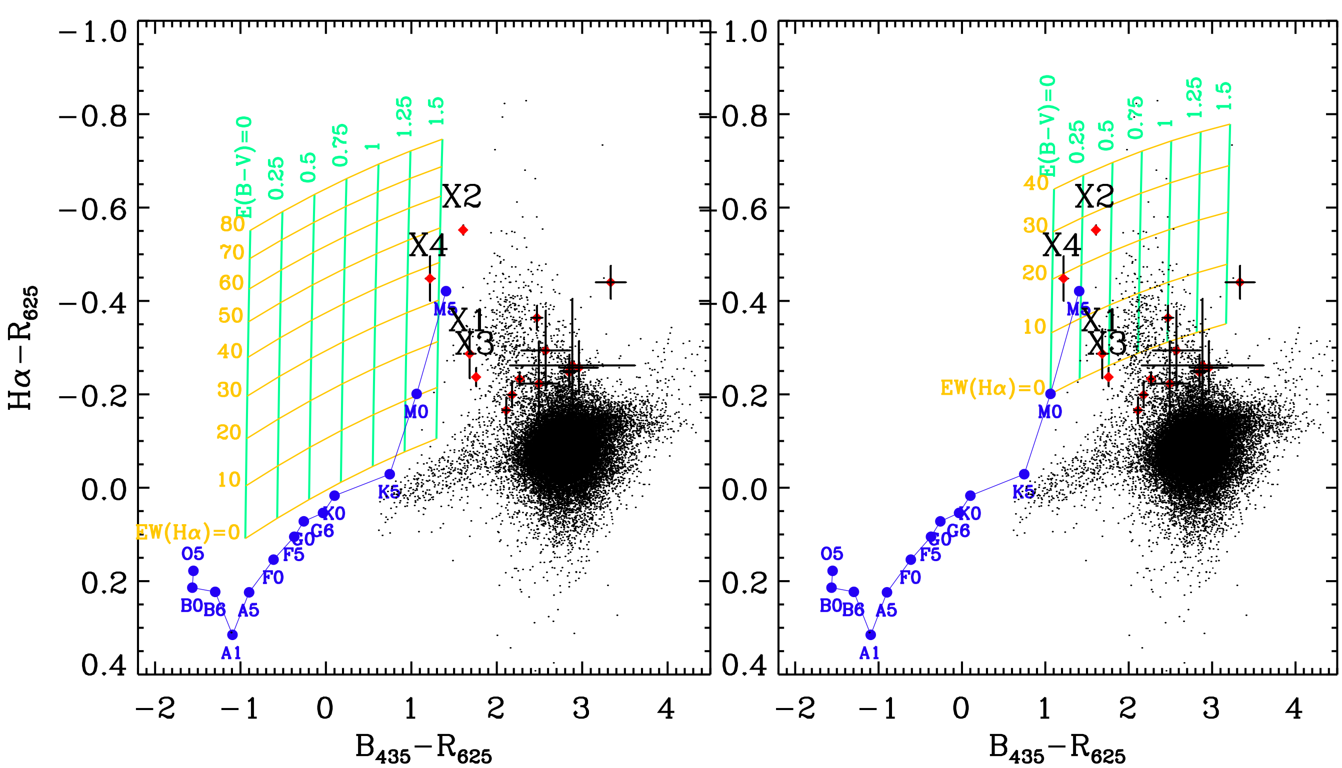


F . 4.— Color-color diagrams with the candidate CVs marked with red diamonds; only the best candidates X 1–4 are labelled. The grids show how the synthetic colors for a disk spectrum (left) and an M0 dwarf spectrum (right) vary as function of reddening $E(B-V)$ and the equivalent width of H$\alpha$. The location of the unreddened main sequence is indicated in blue. We also show the location of the bulk of the ACS sources (for clarity, we only show the sources detected on one of the chips of the mosaic).

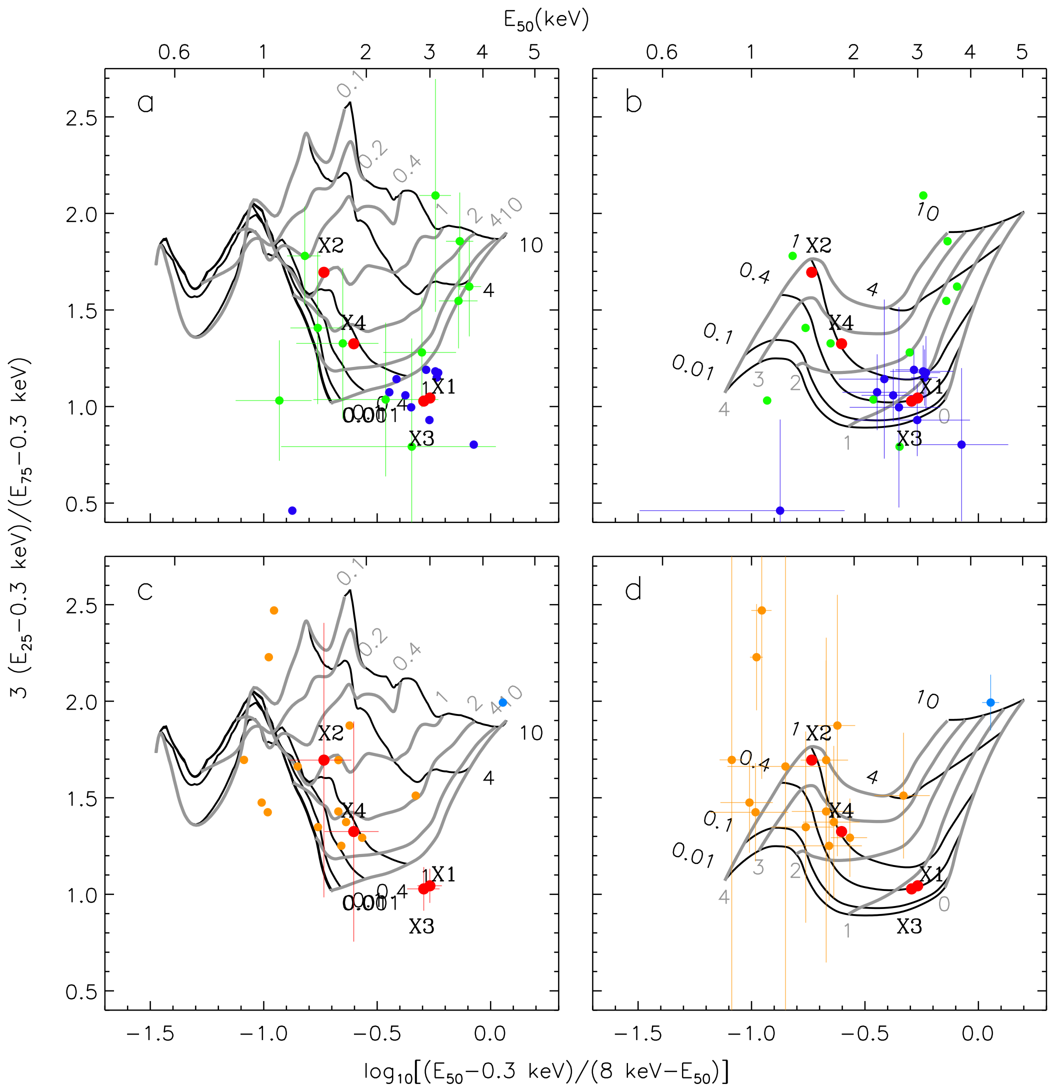


F . 5.— Quantile color-color diagrams with our best candidate CVs X 1–4 marked in each panel with filled red circles. The model grids on the left are computed for a single-temperature MeKaL model, while the grids on the right are for a power-law spectrum. In panels *a* and *b*, we also include the other candidate CVs: in green we show the sources with a small H$\alpha$ excess and in dark blue the sources with a high $f_{Bx}/f_R$ ratio. In panels *c* and *d*, we include the identifications with coronal sources and the absorbed galaxy (§4.2) to compare the X-ray spectra of different source classes. Error bars are plotted in one panel only for clarity. Thick grey lines are contours of constant temperature $kT$ or photon index Γ; black lines are contours of constant $n_H$. Sources with <5 net counts are omitted.

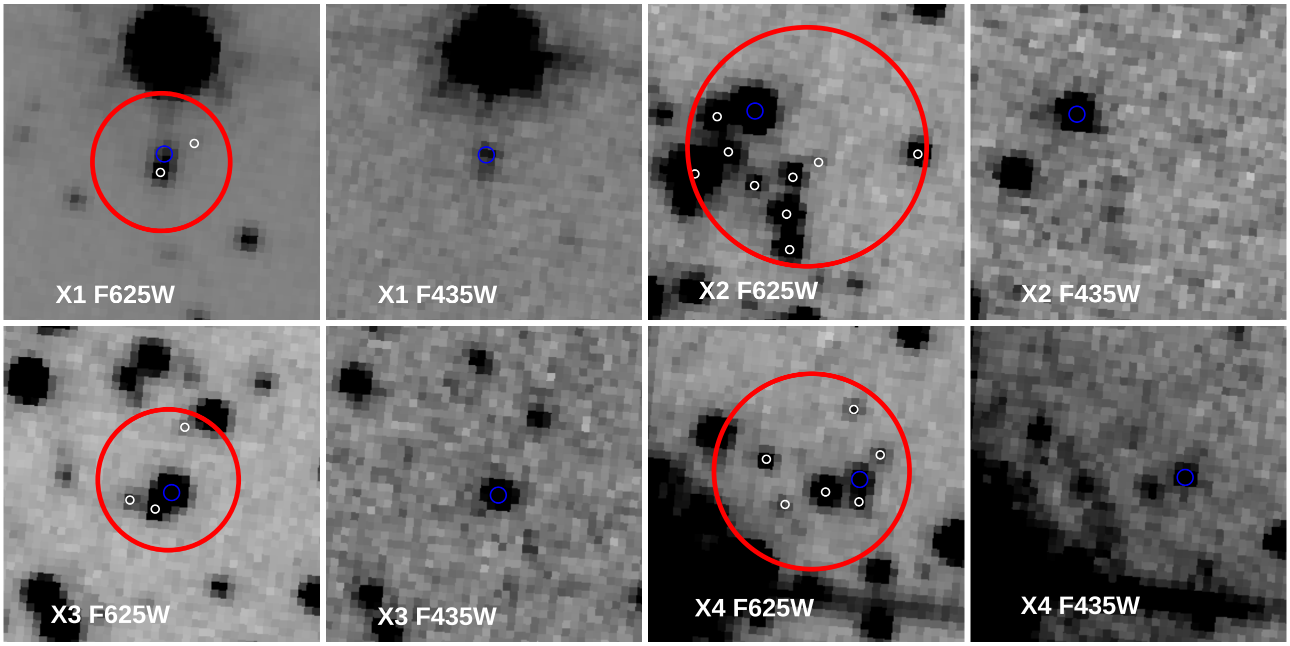


FIG. 6.— Finding charts in F625W and F435W for the four candidate CVs. In the red images, we show the $2\sigma$ search with a red circle (0.″44 for X 1, 0.″76 for X 2, 0.″45 for X 3 and 0.″62 for X 4) and mark the optical sources with small white circles. The candidate CVs are marked with blue circles in all images. The scaling of the images is adjusted to highlight the relatively blue color of the X 1–4. North is up, east to the left.

ing two UCAC2 stars. Since these stars are heavily saturated in the ACS images, it is impossible to look for other optical sources within the error radius; in the field-of-view of the ACS images, stars of this brightness are however rare and we believe that chance alignments are unlikely. Other likely coronal sources are found among astrometric matches of *Chandra* sources to OGLE-III variables (A. Udalski, private communication); while we have not yet done a test to estimate how many of the twelve matches in the ACS field-of-view could be spurious, a detailed analysis of matching the *Chandra* sources in the two other *Windows* with OGLE-II variables (van den Berg et al. 2006) showed that <10% of the matches are expected to be random. Also, some of the light curves vary periodically and suggest binary periods from hours up to tens of days—in line with the detection of X-rays generated by tidally induced rapid rotation. Both the bright sources and the variables are predominantly soft in X-rays and have derived $n_H$ values consistent with the maximum $n_H$ towards *LW* or lower; they occupy a distinctly different region of the CMD than most of the candidate CVs from §4.1.

Another interesting identification is the match of source CXOPS J175137.4-293515 (61±9 net counts) with a red, extended object, see Fig. 7. The quantile diagram suggests that it is highly absorbed and that the spectrum is consistent with a power law with photon index 1–2. We suggest that this source is a type-II AGN, and that some sources (but not all, see §5.3) in this region of the quantile diagram are too.

### 4.3. *Constraints on the hard (2-8 keV) source population*

H08 use the number-density versus flux distribution (logN-logS) of *Chandra* sources in seven inner-bulge fields (including the three *Windows*) to study the hard (2-8 keV) point-source population and its radial distribution in the central region of the Galaxy. Their results suggest that the high concentration of hard sources around SgrA* seen by Muno et al. (2003) is part of a population that extends at least out to *LW* where the hard-source density is still significantly elevated above the extra-galactic logN-logS curve, in contrast to what

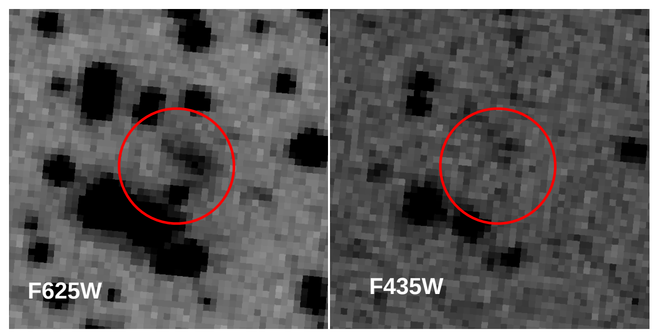


FIG. 7.— Finding charts in F625W and F435W of the region around source CXOPS J175137.4-293515. An extended and red object lies near the center of the $2\sigma$ search readius indicated with the red circle.

is seen in most other Galactic-plane fields. Of the *LW* sources with $\mathrm{SNR}_{Hc}>3$ that are used in the logN-logS analysis by H08, 29 are covered by the ACS mosaic. The corresponding flux limit for a $\mathrm{SNR}_{Hc}=3$ detection is $2\ 10^{-15}$ erg s$^{-1}$ cm$^{-2}$ (2-8 keV; value is averaged over the ACS field-of-view), where we assumed an underlying spectrum with a $\Gamma=1.7$ power-law slope absorbed by $n_H=7.6\ 10^{21}$ cm$^{-2}$ (corresponding to the adopted maximum $A_V$ towards *LW*). Based on the high-latitude hard-source density from Kim et al. (2007), we expect that $\sim$17±4 (poissonian errors only) hard sources are background galaxies. Here we explore what constraints we can set on the nature of the remaining, i.e. Galactic, sources based on our optical identifications.

Of the 29 sources, we have plausible identifications for five: two are identified with optical variables (these are the "softest" hard sources), two are our likely CVs X 1 and X 3, and one is the extended object and probable galaxy. In addition, one of the six optical sources that is matched with CXOPS J175127.8-293510 (28±7 net counts) is exceptionally red with $B_{435}-R_{625}\approx4.7$ but a normal H$\alpha-R_{625}$ color. Such a red color is not expected for stellar sources (see Fig. 4); since there is no H$\alpha$ excess and since the X-ray quantiles show no sign of internal absorption that also could make the optical source look red instead of blue as expected for accreting binaries, this explanation seems also unlikely. We suggest that an active galaxy is the best explanation. For ten more sources, we have ambiguous clues to their origin from the optical: a coronal nature is excluded for six sources with high values for their minimum $f_{Bx}/f_R$ (X 17, X 18, X 19, X 21, X 22, X 25), and four sources matched with objects with small H$\alpha$-excesses (X 5, X 8, X 10, X 14) are also unlikely to be coronal as they have quantile spectral class 2, i.e. all show indications of extra absorption in X-rays. However, as outlined in § 4.1.1 and § 4.1.2, the discriminating properties of these two groups still leave open the possibility that they are either accreting binaries or background galaxies. We have no obvious optical clues for the remaining thirteen sources that all have at least one astrometric match with non-distinct colors; possibly, the true counterpart is too faint to be detected or below the detection limit in at least one band which prevents us from measuring colors. In summary, the only constraint that we can set on the Galactic hard source population is that they are a mix of coronal and accreting sources but are, not unexpectedly, dominated by the latter.

## 5. DISCUSSION

Our search for CVs in *LW* has resulted in three or four plausible systems (X 1 to X 4) and 22 more marginal candidates (X 5 to X 26). In this section we set constraints on the distances of the four best candidates (§5.1), and discuss the CV space density in the bulge (§5.2). We discuss our identifications in the context of hard X-ray sources in the central bulge in §5.3.

### 5.1. *Distance constraints for the CV candidates*

Given the limited information on our candidate CVs, it is a challenge to put meaningful constraints on their distances. With the $R_{625}$ and H$\alpha$ magnitudes, we estimate their minimum distances using the empirical relation between the equivalent width of the H$\beta$ emission line, EW(H$\beta$), and the absolute $V$ magnitude of the accretion disk: EW(H$\beta$)=0.3 $M_V^2$+exp(0.55 ($M_V$-4)) (Patterson 1984). Whereas we do not have direct measurements of the strength of H$\beta$ in our systems, a safe upper limit for EW(H$\beta$) is EW(H$\alpha$); comparing the spectroscopically-determined equivalent widths of these lines in the SDSS CVs (reported in Szkody et al. (2002) and follow-up papers), we find that EW(H$\alpha$) exceeds EW(H$\beta$) in 95% of 197 cases (the mean ratio of EW(H$\beta$) to EW(H$\alpha$) is 0.58 with a standard deviation 0.38). The candidate CV with the largest EW(H$\alpha$) is X 2: its location with respect to the grid in Fig. 4 implies EW(H$\alpha$)≈50Å. For EW(H$\beta$)≤EW(H$\alpha$), it follows that $M_V$≤9.6. Taking into account the distance-dependent reddening from D03, we find $d_{\rm min}$≈1.6 kpc ($V$–$R_{625}$=0) or $d_{\rm min}$≈ 2.2 kpc ($V$–$R_{625}$=1). The other three CV candidates have lower values for EW(H$\alpha$) and their minimum distances determined with this method are accordingly larger ($d_{\rm min}$ is between 3.5 and 5.5 kpc for $V$–$R_{625}$=0, and between 4.4 and 7.7 kpc for $V$–$R_{625}$=1). This suggests that our CV candidates are typically much farther away than the majority of currently known CVs in the field. There are a few caveats however: our value for EW(H$\alpha$) is based on photometry and depends on the model for the underlying optical spectrum. For this we have used a power-law model which is appropriate for disk-dominated systems; if instead the white-dwarf spectrum—with typically broad Balmer absorption lines—contributes significantly around H$\alpha$, our derived EW(H$\alpha$) will be underestimated (and the minimum distances overestimated). Also, the EW(H$\beta$)–$M_V$ relation applies to systems with disks, and is not appropriate for magnetic systems in which no disks or truncated disks are formed.

Another approach to constrain the distances of our candidate CVs is to test the hypothesis that they are at similar distances than most known CVs. The recent study by Ak et al. (2008) suggests that the majority of the latter are closer than ~2 kpc, therefore we ask: based on the local CV space density, how many CVs are expected within the volume inside $d$=2 kpc and the field-of-view of the ACS mosaic? To answer this question, we integrate the CV space density $n_{\rm CV}$ along the line of sight and assume for its variation as a function of distance an exponential-disk model with a vertical scale height of 200 pc and a radial scale length of 2.5 kpc (other galactic components, e.g. a bulge, are not relevant when relatively short distances are considered). The resulting number of CVs contained in this volume, regardless of the selection effects that these systems would be subjected to in order to be detected in our sample, is 0.15 and 0.44 for a local CV density 1 $10^{-5}$ and 3 $10^{-5}$ systems pc$^{-3}$, respectively (Ak et al. 2008; Grindlay et al. 2005). We conclude that it is unlikely that all our candidate CVs are part of the known local population and that instead we have probed the CV population at distances larger than ~2 kpc.

### 5.2. *The CV density in the bulge*

Since we can derive only very crude distances for our candidate CVs, it is not possible to use them for constraining the bulge CV density. Instead, we assume that beyond the local neighborhood the ratio of the CV space density to the stellar space density is the same as locally, and compare the number of CVs we expect to detect based on this assumption with the number we actually see. Given the small statistics of our sample, we are not able to set strong contraints on the bulge CV density.

We start by calculating the number of stars that are included in a volume subtended by the 6.′5×6.′5 field-of-view of the ACS mosaic. We use the Galaxy model by Picaud & Robin (2004) which consists of two parts. The first is a multi-component disk with a radial scale length of 2.35 kpc, a vertical scale height between 60 and 185 pc (depending on the age of the disk component) and a central hole with a scale length of 1.31 kpc, while the second component is a triaxial bulge with a major axis of 1.82 kpc, axis ratios of approximately 1:0.31:0.26, and a major axis that is rotated with respect to the line connecting us and the Galactic Center by ~11°; see Picaud & Robin (2004) for detailed parameters of this model (sech$^2$ density profile and Pad7.9 luminosity function). The star densities are normalized such that the disk component gives a local star density of 0.145 stars pc$^{-3}$ and that the bulge has 11.5 stars pc$^{-3}$ in the center of the Galaxy. Integrating this model along the line of sight up to the maximum distance $d_{\rm max}$ at which we can detect CVs (38 kpc for the brightest CVs with $M_V$=+3, Patterson (1998)) gives a total of 11 $10^6$ stars. Assuming that throughout this volume the ratio of CVs to stars is the same as the local value (6.8 $10^{-5}$ for a local CV space density of 1 $10^{-5}$, see Grindlay et al. (2005)) implies that there are ~770 CVs in this volume.

We verify how well the number of stars predicted by the model compares to the number that is actually observed. To account for the dependence of the distance out to which stars of different masses can be detected, we fold the Galaxy model with the local luminosity function from Bahcall & Soneira (1980). To reduce incompleteness effects in our data as much as possible we calculate the number of stars expected to be detected between $V$=18 and $V$=24. For simplicity, we neglect differences between the luminosity functions in the $V$ and $R_{625}$ bands which we believe are modest: the stars that dominate the optical detections are of spectral types A to K which have $V-R<1$. We find that approximately six times more stars are predicted than we observe in the $R_{625}$ images. For now we do not explore in detail the origin(s) of this discrepancy (the galaxy model, uncertainties in $A_V$ or variations in $A_V$ across the field-of-view, detection incompleteness); we simply reduce the number of expected CVs by this factor, which results in ∼120 CVs expected.

Not all CVs will be detectable given the limits of our X-ray and optical observations. We simulate our detection efficiency with a similar technique as used by Koenig et al. (2008), with the biggest difference a more detailed Galaxy model and the incorporation of the bulge. We create a sample of $10^6$ fake CVs to which we randomly assign an X-ray luminosity and $f_{Bx}/f_R$ ratio based on the observed distributions in the sample of Verbunt et al. (1997), and a distance somewhere between us and $d_{\max}$. The number of fake CVs as a function of distance is proportional to the CV density at a given distance and the integration area subtended by the ACS mosaic at that distance. We assume that the CV space density follows the same profile as the Picaud & Robin (2004) Galaxy model but scale the normalization to match it to the local CV density of 1 $10^{-5}$ CVs $\mathrm{pc}^{-3}$ (Grindlay et al. 2005). Furthermore, we assume the D03 model for $A_V$ as function of distance, again scaled to match M06 at 8 kpc (§3.3). For each fake CV we then asses whether it falls above the detection limit in the ACS images (we use $R_{625}$=24, slightly fainter than X 1 and X 4; below that limit the three-band detections become incomplete) and in the *Chandra* data (we use a 10-keV thermal-bremsstrahlung spectral model and a fluxlimit corresponding to a SNR=3 detection). The resulting detection efficieny is 20%, This number does not depend much on the choice of X-ray spectral model (a 5-keV thermal bremsstrahlung gives a very similar result), but it is sensitive to $A_V$: an increase in $A_V$ by 25% reduces the efficiency to 15%, while a decrease in $A_V$ by 25% gives an efficiency of 27%. The simulated efficiency is still an upper limit to the real efficiency. For example, a fraction of CVs have no or weak H$\alpha$ emission lines (e.g. dwarf novae in outburst) and would consequently not be selected as plausible CVs. Also, CVs that do not stand out as blue sources like X 1–4 (e.g. as a result of internal absorption or high $A_V$) will be counted as marginal candidates.

In summary, the predicted number of CVs is at most ∼0.2×120=24, compared to three to four observed good candidates and almost two dozen possible CVs and marginal candidates. At face value, this implies that the bulge relative CV density is similar to or lower than the local value. In light of the many uncertainties (X-ray luminosity and $f_x/f_V$ distributions, extinction, X-ray and optical spectral properties, Galactic distribution) and the small observed sample, we cannot draw any firm conclusions. In a follow-up paper where we report on the search for candidates CVs in the other two *Window* fields, the constraints on the bulge CV density will be reconsidered with improved statistics.

### 5.3. *The hard X-ray sources in the central bulge*

We have found two plausible accreting binaries among the hard sources in *LW*. The hardness of their X-ray spectra as inferred from X-ray quantiles (power-law photon indices $\Gamma<1$, see Fig. 5) suggests the properties of X 1 and X 3 are consistent with those of magnetic CVs, the source class that has been suggested to dominate the hard source population in the Galactic-Center region. Since the radial-distribution analysis by H08 suggests that it extends at least out to *LW*, X 1 and X 3 could be the first optically identified members of this population. Not one of the hard sources in *LW* matches with a bright ($R_{625}$<17) optical source, which supports the conclusion by Laycock et al. (2005) that this population is not dominated by wind-fed Be high-mass X-ray binaries. Indeed, their bright companions cannot be missed: a typical B0V secondary with $M_V=-4$, $V-R\approx-0.1$ and seen through $A_V$=4.2, would have $R_{625}\approx14.5$ at 8 kpc and $R_{625}\approx16.3$ at twice that distance.

Not unexpectedly, the comparsion of the X-ray spectral properties of the hard sources in the central-bulge fields shows a steady increase of $n_H$ when moving closer to the Galactic Center (H08). More surprising is that the number of sources with $n_H$ greater than a few times $10^{22}$ $\mathrm{cm}^{-2}$ already starts to rise when moving from Baade's Window to *LW*—the maximum value of $n_H$ towards these fields is indeed smaller than this value. Since no increase in the number of extra-galactic sources is expected between the fields, the extra absorbed sources must be of Galactic origin. Among them, we have identified several that are matched with optical sources with a small H$\alpha$ excess. If the origin of this excess is an accretion disk or stream, then the fact that the optical sources do not stand out in their $B_{435}-R_{625}$ color could be explained if the optical light is partially subject to extra absorption as well. Examples of internally absorbed accreting binaries are, again, magnetic CVs but also the new class of high-mass X-ray binaries discovered by *INTEGRAL* that are enshrouded in the strong wind of the secondary (Chaty 2008).

## 6. CONCLUSIONS

We have conducted a search for CVs in a low-extinction bulge field at 1$^{\mathrm{d}}$.5 angular separation from the Galactic Center. This has resulted in the discovery of three to four probable CVs and 23 additional candidates that could also be coronally active stars or background galaxies. We argue that the distances of the best candidates are ≳2 kpc and use this to investigate the CVs space density in the bulge. Despite the many uncertainties in the properties of the Galactic CV population and despite our small sample, we find no huge discrepancy between the number of observed and expected systems based on a constant ratio of CV to stars throughout the Galaxy (fixed at the local value). We will address this issue in more detail with similar studies in other low-extinction bulge fields.

If the Galactic-Center hard X-ray source population extends out to the field studied in this paper, as suggested by H08, two of our plausible CVs could be the first optically identified members of this elusive population and more may be present among our our other CV candidates. This makes the sources presented in this paper prime targets for more investigations. We can only extract limited information from our three-band ACS images. Ground-based optical spectroscopy will be impossible for some candidates (like X 1) but we encourage follow-up work on the more isolated ones. With the deeper (∼900 ks) *Chandra* observations of *LW*, the X-ray spectral properties and temporal variability of the sources can be studied in more detail allowing one to place better constraints on their nature.

This work is supported by Chandra grants G03-4033A and AR6-7010X.

## REFERENCES

Ak, T., Bilir, S., Ak, S., & Eker, Z. 2008, New Astronomy, 13, 133
Bahcall, J. N., & Soneira, R. M. 1980, ApJS, 44, 73
Chaty, S. 2008, ArXiv e-prints, 805
Dempsey, R. C., Linsky, J. L., Fleming, T. A., & Schmitt, J. H. M. M. 1993, ApJSS, 86, 599
Dempsey, R. C., Linsky, J. L., Fleming, T. A., & Schmitt, J. H. M. M. 1997, ApJ, 478, 358
Dolphin, A. E. 2000, PASP, 112, 1383
Drew, J. E. et al. 2005, MNRAS, 362, 753
Drimmel, R., Cabrera-Lavers, A., & López-Corredoira, M. 2003, A&A, 409, 205
Grindlay, J. et al. 2005, ApJ, 635, 920
Güdel, M. 2004, A&A Rev., 12, 71
Hong, J., Grindlay, J., van den Berg, M., Zhao, P., & Laycock, S. 2008, ApJ (submitted)
Hong, J., Schlegel, E. M., & Grindlay, J. E. 2004, ApJ, 614, 508
Hong, J., van den Berg, M., Schlegel, E., Grindlay, J., Koenig, X., Laycock, S., & Zhao, P. 2005, ApJ, 635, 907
Kim, M., Wilkes, B. J., Kim, D.-W., Green, P. J., Barkhouse, W. A., Lee, M. G., Silverman, J. D., & Tananbaum, H. D. 2007, ApJ, 659, 29
Koekemoer, A., McLean, B., McMaster, M., & Jenkner, H. 2005, Instrument Science Report ACS 2005-06, Tech. rep., STScI
Koenig, X., Grindlay, J. E., van den Berg, M., Laycock, S., Zhao, P., Hong, J., & Schlegel, E. M. 2008, ApJ (in press)
Krautter, J. et al. 1999, A&A, 350, 743
Laycock, S., Grindlay, J., van den Berg, M., Zhao, P., Hong, J., Koenig, X., Schlegel, E. M., & Persson, S. E. 2005, ApJ, 634, L53
Marshall, D. J., Robin, A. C., Reylé, C., Schultheis, M., & Picaud, S. 2006, A&A, 453, 635
Mochnacki, S. W. et al. 2002, AJ, 124, 2868
Muno, M. P. et al. 2003, ApJ, 589, 225
Osten, R. et al. 2008, The Astronomer's Telegram, 1499, 1
Patterson, J. 1984, ApJS, 54, 443
—. 1998, PASP, 110, 1132
Pfahl, E., Rappaport, S., & Podsiadlowski, P. 2002, ApJ, 571, L37
Picaud, S., & Robin, A. C. 2004, A&A, 428, 891
Predehl, P., & Schmitt, J. H. M. M. 1995, A&A, 293, 889
Schmitt, J. H. M. M., & Liefke, C. 2004, A&A, 417, 651
Sirianni, M. et al. 2005, PASP, 117, 1049
Stocke, J. T., Morris, S. L., Gioia, I. M., Maccacaro, T., Schild, R., Wolter, A., Fleming, T. A., & Henry, J. P. 1991, ApJS, 76, 813
Szkody, P. et al. 2002, AJ, 123, 430
van den Berg, M. et al. 2006, ApJ, 647, L135
Verbunt, F., Bunk, W. H., Ritter, H., & Pfeffermann, E. 1997, A&A, 327, 602
Warner, B. 1995, Cataclysmic variable stars (Cambridge Astrophysics Series, Cambridge, New York: Cambridge University Press, —c1995)
Zacharias, N., Urban, S. E., Zacharias, M. I., Wycoff, G. L., Hall, D. M., Monet, D. G., & Rafferty, T. J. 2004, AJ, 127, 3043
Zhao, P., Grindlay, J., Hong, J., Laycock, S., Koenig, X., Schlegel, E., & van den Berg, M. 2005, ApJS, 161, 429